

Spin-orbit coupling and vibronic effects on spectroscopic properties of metal complexes

Herbert D. Ludowieg

Department of Chemistry, University at Buffalo, State University of New York

April 17, 2023

Outline

1

Introduction

- Forbidden transitions
- Vibrational Raman Optical Activity
- Induced Optical Activity

2

Optical Activity of Spin-Forbidden Transitions

3

Raman Optical Activity of $[M(en)_3]^{3+}$

4

Vibronic absorption spectra $[UX_6]^{2-}$

5

Magnetochiral Dichroism of $[Ni(en)_3]^{2+}$

Outline for section 1

1

Introduction

- Forbidden transitions
- Vibrational Raman Optical Activity
- Induced Optical Activity

2

Optical Activity of Spin-Forbidden Transitions

3

Raman Optical Activity of $[M(en)_3]^{3+}$

4

Vibronic absorption spectra $[UX_6]^{2-}$

5

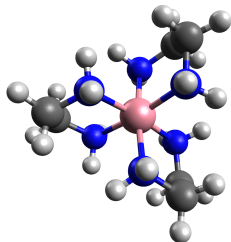
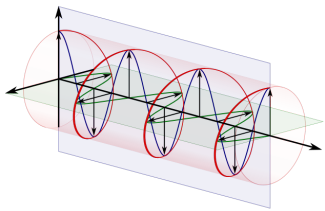
Magnetochiral Dichroism of $[Ni(en)_3]^{2+}$

Forbidden transitions and selection rules

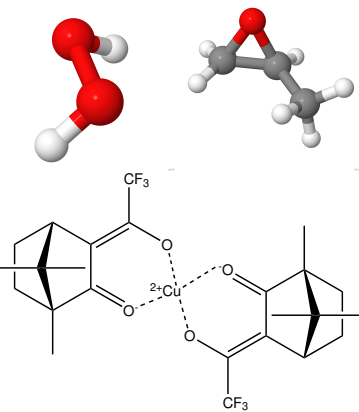
- Selection rules govern the ability of an electron to transition between states
- Laporte selection rule states that a transition between two states must have a change in parity
- A spin-forbidden transition is one involving two states of different multiplicities
- In order to calculate the intensities in spin-forbidden transitions relativistic spin-orbit effects have to be introduced

Vibrational Raman optical activity (VROA)

- VROA is among the most recently developed chiroptical methods
- Measures the difference between left-/right-circularly polarized inelastically scattered light
- ROA studies have been found in protein structure analysis and transition metal complexes



- Nafie¹ developed a two-state model where the resonance ROA intensities become mono-signate
- Confirmed by Jensen, et al² for H₂O₂ and (S)-methyloxirane
- Merten, et al³ found that for bis-(trifluoroacetylcamphorato)copper(II) the RROA spectrum remains bi-signate



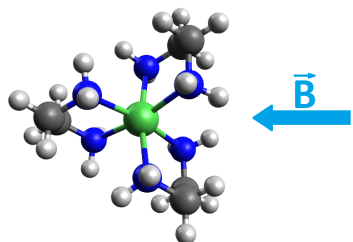
¹ Nafie, et al *Chem. Phys.* **1996**, *205*, 309–322

² Jensen, et al *J. Chem. Phys.* **2007**, *127*, 134101

³ Merten, et al *J. Phys. Chem.* **2012**, *116*, 7329–7336

Induced OA

- It is possible to induce OA on molecules by applying an external magnetic field
- Common application is magnetic circular dichroism (MCD)
- MCD is similar to natural CD (NCD) where the differential absorption of left-/right-circularly polarized light is measured
- No information regarding the absolute configuration can be extracted



Magnetochiral dichroism (MChD)

- Unlike MCD, MChD was developed as an enantioselective technique
- Unlike MCD and NCD, the propagated light can be unpolarized
- Performing accurate measurements of MChD proves difficult as the MCD and NCD effects in the NIR region are much more dominant
- Will show that we get good agreement of the MChD spectra of $[\text{Ni}(\text{en})_3]^{2+}$ to experiment

Outline for section 2

1 Introduction

- Forbidden transitions
- Vibrational Raman Optical Activity
- Induced Optical Activity

2 Optical Activity of Spin-Forbidden Transitions

3 Raman Optical Activity of $[M(en)_3]^{3+}$

4 Vibronic absorption spectra $[UX_6]^{2-}$

5 Magnetochiral Dichroism of $[Ni(en)_3]^{2+}$

- Dipole and rotatory strengths

$$D = \langle \Psi_n | \hat{\mathbf{d}} | \Psi_m \rangle \cdot \langle \Psi_m | \hat{\mathbf{d}} | \Psi_n \rangle$$

$$R = \text{Im} \left[\langle \Psi_n | \hat{\mathbf{d}} | \Psi_m \rangle \cdot \langle \Psi_m | \hat{\mathbf{m}} | \Psi_n \rangle \right]$$

$$\hat{\mathbf{m}} = -\mu_B (\hat{\mathbf{L}} + 2\hat{\mathbf{S}}) \quad \hat{\mathbf{d}} = -e\hat{\mathbf{r}}$$

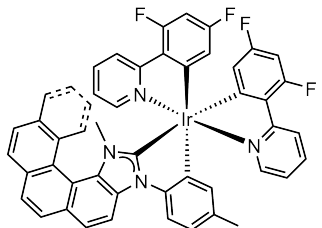
- Dissymmetry factor, radiative decay constant, and oscillator strength

$$g_{\text{lum}} = 4R/D$$

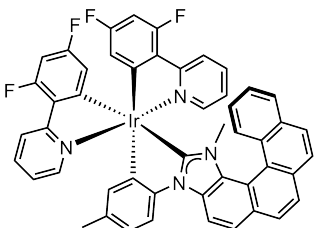
$$k = 2\alpha^3 n^2 E^2 f$$

$$f = \frac{2}{3} \Delta E_{n,m} D$$

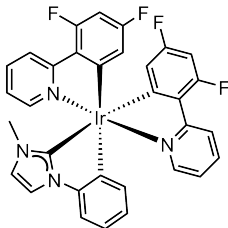
Molecules studied



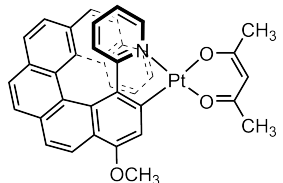
$(P,\Delta_{\text{Ir}})\text{-A}^1$



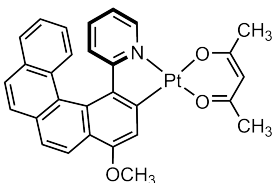
$(P,\Delta_{\text{Ir}})\text{-A}^2$



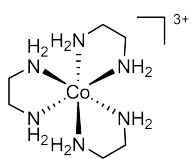
$\Delta_{\text{Ir}}\text{-A}$



$P\text{-3a}$



$P\text{-3c}$



$\Delta\text{-}[\text{Co}(\text{en})_3]^{3+}$

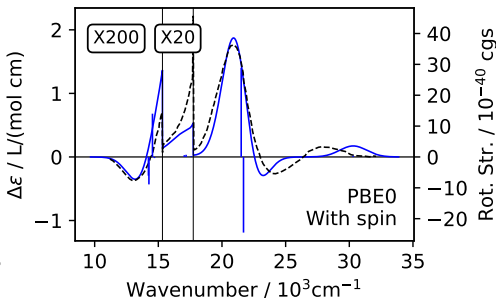
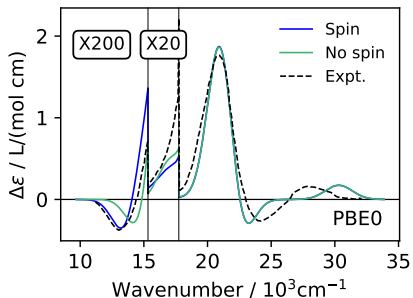
Computational Details

- The Ir and Pt complexes were optimized with scalar ZORA spin-unrestricted DFT, employing the PBE0 functional
- The TZ2P basis set was used for the metals, DZ on the hydrogen and DZP for everything else
- TD-DFT calculations employed a COSMO for dichloromethane and the TDA with the PBE0 functional
- $[\text{Co}(\text{en})_3]^{3+}$ was optimized with the B3LYP functional
- TD-DFT calculations employed the TDA with the PBE0 functional
- The four distinct conformers of $[\text{Co}(\text{en})_3]^{3+}$ were within 1 kcal/mol
- Use of the TDA takes care of triplet instabilities in agreement with observations by Peach, et. al.⁴

⁴ Peach; et al, *J. Chem. Theory Comput.* **2011**, 7, 11, 3578–3585

$(P, \Lambda_{lr})-\mathbf{A}^1$	$(P, \Delta_{lr})-\mathbf{A}^2$	$\Lambda_{lr}-\mathbf{A}$	$P-3\mathbf{a}$	$P-3\mathbf{c}$
Experimental data				
$\tau / \mu\text{s}$	350	280	0.53 / 2.4 ^a	16.5
$g_{lum} \times 10^{-3}$	3.7	1.5	-0.9	4.0
Calcd. TDA-TD-DFT/PBE0				
$\tau / \mu\text{s}$	452	417	3.9	92.7
$g_{lum} \times 10^{-3}$	0.0812	2.07	-1.08	-0.754
No spin				
$g_{lum} \times 10^{-3}$	1.24	2.81	-1.46	2.21
Spin				

^a Observed decay kinetics was bi-exponential at room-temperature.



- $\text{[Co(en)}_3]^{3+}$ ECD spectra PBE0-TDA//B3LYP
- Experimental spectrum (dashed lines) from Mason and Peart⁵
- No shift was applied to the data
- Used a gaussian broadening of 2500 cm^{-1} (0.31 eV)

⁵ Mason; Peart, *J. Chem. Soc. Dalton Trans* **1977**, 9, 937–941

Outline for section 3

1 Introduction

- Forbidden transitions
- Vibrational Raman Optical Activity
- Induced Optical Activity

2 Optical Activity of Spin-Forbidden Transitions

3 Raman Optical Activity of $[M(en)_3]^{3+}$

4 Vibronic absorption spectra $[UX_6]^{2-}$

5 Magnetochiral Dichroism of $[Ni(en)_3]^{2+}$

Vibrational Raman Optical Activity

- The ROA intensities for a backscattering setup are calculated by

$$I^R(180^\circ) - I^L(180^\circ) = \Delta \frac{d\sigma}{d\Omega}(180^\circ) = K_p \left[\frac{48(\beta(G')_p^2 + \beta(A)_p^2/3)}{90c} \right]$$

$$\beta(G')_p^2 = \text{Im} \left(i \frac{3\alpha_{\alpha\beta}^p G'^{p*}_{\alpha\beta} - \alpha_{\alpha\alpha}^p G'^{p*}_{\beta\beta}}{2} \right)$$

$$\beta(A)_p^2 = \text{Re} \left(\frac{1}{2} \omega \alpha_{\alpha\beta}^p \epsilon_{\alpha\gamma\delta} A_{\gamma\delta\beta}^{p*} \right)$$

$$K_p = \frac{\pi^2}{\epsilon_0^2} (\tilde{\nu}_{\text{in}} - \tilde{\nu}_p)^4 \frac{h}{8\pi^2 c \tilde{\nu}_p} \frac{1}{1 - \exp[-hc\tilde{\nu}_p/k_B T]}$$

Vibrational Raman optical activity

- The transition tensors can be expressed as geometric derivatives of the molecular properties

$$\Theta^p \Lambda^p = \langle 0 | \Theta | 1_p \rangle \langle 1_p | \Lambda | 0 \rangle = \frac{\partial \Theta}{\partial Q_p} \Big|_0 \quad \frac{\partial \Lambda}{\partial Q_p} \Big|_0$$

- Θ and Λ can be:
 - $\alpha_{\alpha\alpha}$: dipole-dipole polarizability transition tensor
 - $G'_{\alpha\beta}$: electric dipole-magnetic dipole polarizability transition tensor
 - $A_{\gamma\delta\beta}$: electric dipole-electric quadrupole polarizability transition tensor

$$K_p = \frac{\pi^2}{\epsilon_0^2} (\tilde{\nu}_{\text{in}} - \tilde{\nu}_p)^4 \frac{h}{8\pi^2 c \tilde{\nu}_p} \frac{1}{1 - \exp[-hc\tilde{\nu}_p/k_B T]}$$

- This is an experimental parameter as it depends on the incident frequency, $\tilde{\nu}_{\text{in}}$
- The backscattering intensities are formally calculated as

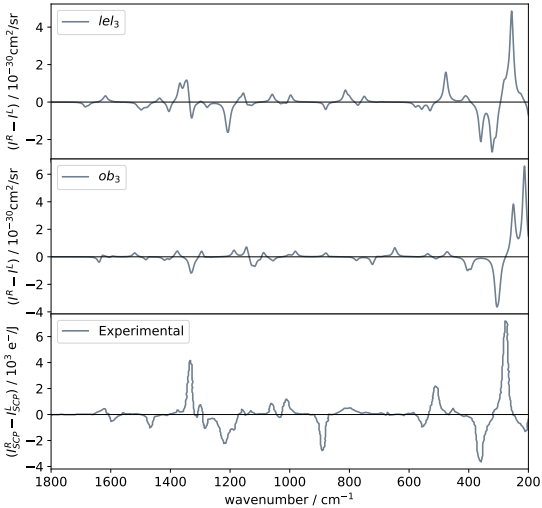
$$\Delta \frac{d\sigma}{d\Omega}(180^\circ) \propto \frac{4}{c} \left[24\beta (G')_p^2 + 8\beta (A)_p^2 \right]$$

ROA calculations

- Optimizations of $[\text{Co}(\text{en})_3]^{3+}$ and $[\text{Rh}(\text{en})_3]^{3+}$ were performed with the Gaussian program package
- A B3LYP hybrid functional along with a def2-TZVP Gaussian-type basis set was used. A 28-electron ECP was used for Rh.
- Linear response tensors were calculated with the KS response module of NWChem
- Calculation of the ROA intensities was performed with newly developed in-house code

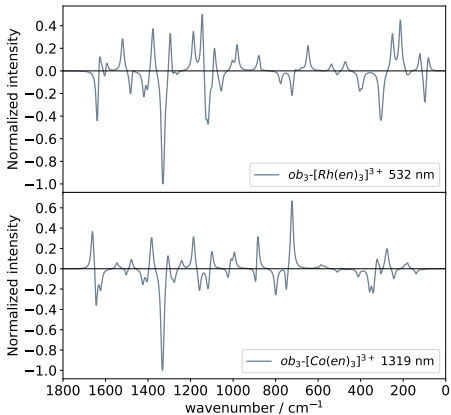
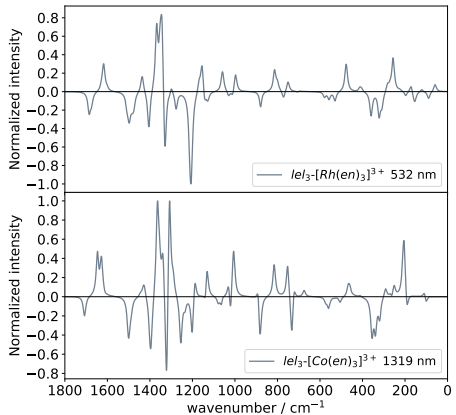
ROA calculations for $[\text{Rh}(\text{en})_3]^{3+}$

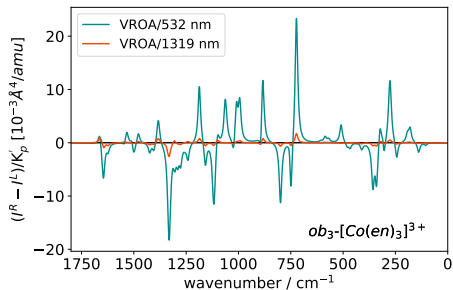
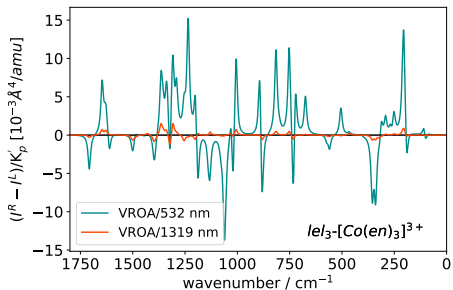
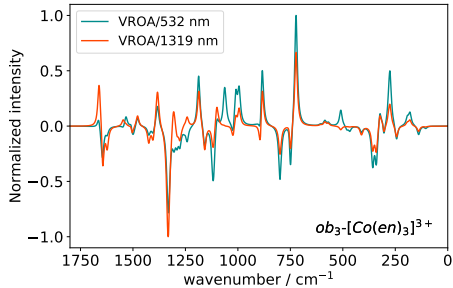
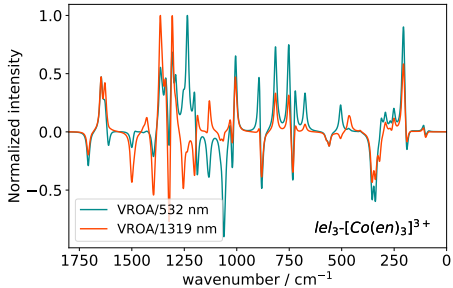
- Calculated at 532 nm (2.331 eV) wavelength
- $|el|_3$ structure agrees well with experimental spectrum
- Agrees with findings by Humbert-Droz, et al⁶



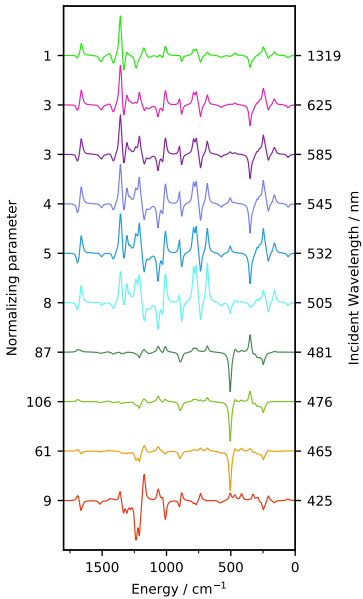
⁶ Humbert-Droz; et al, *Phys. Chem. Chem. Phys.* **2014**, *16*, 23260–23273

- The incident wavelength energy falls far below the lowest electronic excitation energy of $[\text{Rh}(\text{en})_3]^{3+}$ at 320 nm (3.871 eV)
- For $[\text{Co}(\text{en})_3]^{3+}$ the lowest calculated electronic transitions happen at 476 nm (2.605 eV) and 481 nm (2.578 eV)
- The incident laser wavelength falls within the near-resonance domain



a*b*

- Performed a scan of different incident wavelengths from 425 nm to 1319 nm for $[\text{Co}(\text{en})_3]^{3+}$
- All spectra normalized to the strongest peak in the 1319 nm spectrum
- ROA intensities rise sharply as the incident wavelength comes closer to the electronic excitation wavelength⁷



⁷ Abella; Ludowieg; and Autschbach, *Chirality* **2020**, *32*, 741–752

Outline for section 4

1 Introduction

- Forbidden transitions
- Vibrational Raman Optical Activity
- Induced Optical Activity

2 Optical Activity of Spin-Forbidden Transitions

3 Raman Optical Activity of $[M(en)_3]^{3+}$

4 Vibronic absorption spectra $[UX_6]^{2-}$

5 Magnetochiral Dichroism of $[Ni(en)_3]^{2+}$

Born-Oppenheimer approximation

- Central to quantum chemistry
- To a good approximation the electrons can be considered to be moving in a field of fixed nuclei
- Separates the wavefunction into a product of the electronic and nuclear wavefunctions
- Much of computational research is on static systems
- What happens when the nuclei are allowed to move?

$$\Psi(q; Q) = \psi(q; Q) \phi(Q)$$

Vibronic coupling

$$\mu_{1,2} = \langle \Psi_1(q; Q) | \mu | \Psi_2(q; Q) \rangle$$

$$\mu_{1,2} = \langle \phi_1(Q) | \mu_{1,2}^e(Q) | \phi_2(Q) \rangle$$

$$\mu_{1,2}^e(Q) = \langle \psi_1(q; Q) | \mu | \psi_2(q; Q) \rangle$$

$$\langle \phi_1(Q) | \mu_{1,2}^e(Q) | \phi_2(Q) \rangle = \mu_{1,2}^e(Q_0) \langle \phi_1 | \phi_2 \rangle + \sum_p^n \langle \phi_1 | Q_p | \phi_2 \rangle \left. \frac{\partial \mu_{1,2}^e}{\partial Q_p} \right|_0 + \dots$$

- Franck-Condon approximation, $\mu_{1,2}^e(Q_0) \langle \phi_1 | \phi_2 \rangle$
- Herzberg-Teller approximation, $\sum_p^n \langle \phi_1 | Q_p | \phi_2 \rangle \left. \frac{\partial \mu_{1,2}^e}{\partial Q_p} \right|_0$
- In the limit of small approximations

$$\langle \phi_1(Q) | \mu_{1,2}^e(Q) | \phi_2(Q) \rangle = \mu_{1,2}^e(Q_0) \langle \phi_1 | \phi_2 \rangle + \sum_p^n \langle \phi_1 | Q_p | \phi_2 \rangle \left. \frac{\partial \mu_{1,2}^e}{\partial Q_p} \right|_0$$

27/43

Origin of $\partial\mu_{1,2}^e/\partial Q_p$

- Considering a perturbation expansion of the wavefunction to first order

$$\psi_a(q; Q) = \psi_a^0 + \sum_{j \neq a} \psi_a^0 C_{aj}$$

$$C_{aj} = \frac{\langle \psi_a^0 | \partial H / \partial Q | \psi_j^0 \rangle}{E_a^0 - E_j^0} (Q - Q_0)$$

- Following a prescription by Orlandi⁸

$$C_{aj} = \frac{\partial \langle \bar{\psi}_a^0 | H | \bar{\psi}_j^0 \rangle / \partial Q}{E_a^0 - E_j^0}$$

- Where, a ‘floating’ atomic orbital basis is used re-calculating the one- and two-electron integrals at each value of Q keeping the CI coefficients the same as Q_0

⁸ Orlandi, *J. Chem. Phys.* **1976**, 44 277–280

Origin of $\partial\mu_{1,2}^e \partial Q_p$

- Derivative determined by a Sum-over states perturbation theory approach

$$\begin{aligned}\frac{\partial\mu_{1,2}^e(Q)}{\partial Q_p} = & \sum_{k \neq 1} \langle \psi_k^0 | \mu_{1,2}^e | \psi_2^0 \rangle \frac{\partial \langle \bar{\psi}_1^0 | H | \bar{\psi}_k^0 \rangle / \partial Q}{E_1^0 - E_k^0} \\ & - \sum_{k \neq 2} \langle \psi_1^0 | \mu_{1,2}^e | \psi_k^0 \rangle \frac{\partial \langle \bar{\psi}_k^0 | H | \bar{\psi}_2^0 \rangle / \partial Q}{E_k^0 - E_2^0}\end{aligned}$$

- Spin-orbit coupling is introduced via

$$\mu_{1,2}^{\text{SO}} = \sum_{k,m} U_{1,k}^{0\dagger} \langle \phi_k | \mu_{k,m}^{\text{SF}}(Q) | \phi_m \rangle U_{m,2}^0$$

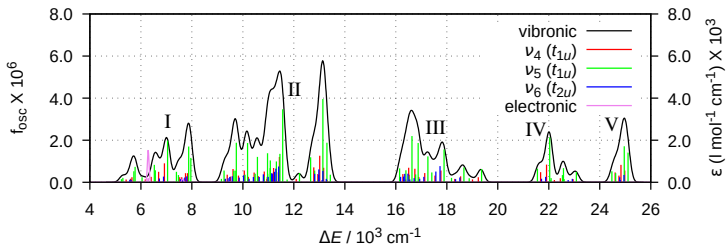
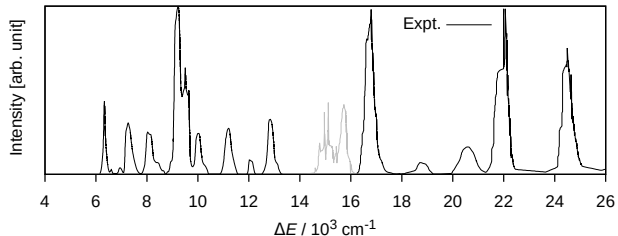
5f-to-5f NIR transitions of $[\text{UX}_6]^{2-}$ ($\text{X} = \text{Cl}, \text{Br}$)

- The transitions in the 5f manifold of $[\text{UX}_6]^{2-}$ ($\text{X} = \text{Cl}, \text{Br}$) are forbidden transitions as the molecule has O_h symmetry
- Due to symmetry all 5f orbitals are of the same parity and Laporte forbidden
- When the molecule distorts higher states will couple and provide intensity borrowing
- Only normal modes that break the inversion symmetry will contribute

Computational Details

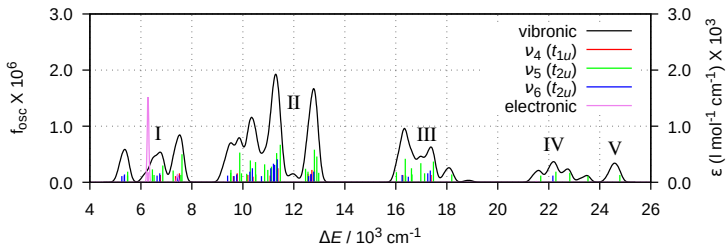
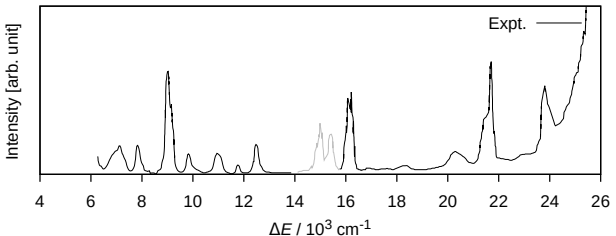
- Kohn-Sham DFT details
 - All calculations were performed with the ADF program suite using the semi-local PBE functional
 - The optimization and harmonic frequency calculations used the TZ2P basis set and the scalar relativistic ZORA Hamiltonian
 - The molecules were calculated in the $a_{2u}^1 t_{2u}^1$ ground state
- Wavefunction theory calculations
 - All calculations were performed with the OpenMolcas program suite
 - Scalar relativistic effects were introduced via the second-order Douglas-Kroll-Hess Hamiltonian
 - ANO-RCC-VTZP basis sets were used
 - MS-PT2 calculations were performed to capture dynamic electron correlation
 - SOC was introduced via restricted active space state interaction
- Post-processing to calculate vibronic intensities was handled by a newly developed code

Results $[\text{UCl}_6]^{2-}$



⁸ Ryan; Jørgensen, *Mol. Phys.*, **1964**, 7, 17–29

Results $[\text{UBr}_6]^{2-}$



⁸ Ryan; Jørgensen, *Mol. Phys.*, 1964, 7, 17–29

Outline for section 5

1 Introduction

- Forbidden transitions
- Vibrational Raman Optical Activity
- Induced Optical Activity

2 Optical Activity of Spin-Forbidden Transitions

3 Raman Optical Activity of $[M(en)_3]^{3+}$

4 Vibronic absorption spectra $[UX_6]^{2-}$

5 Magnetochiral Dichroism of $[Ni(en)_3]^{2+}$

Magneto Chiral Dichroism intensities

- Theory for MChD was developed by Barron and Vrbancich⁹

$$\Delta n_{\text{MChD}}^{\text{D/L}}(\omega, \mathbf{k}, \mathbf{B}) \propto \mathbf{k} \cdot \mathbf{B} \left[A_1^{\text{D/L}} \cdot f_1(\omega) + \left(B_1^{\text{D/L}} + C_1^{\text{D/L}}/kT \right) g_1(\omega) + A_2^{\text{D/L}} \cdot f_2(\omega) + \left(B_2^{\text{D/L}} + C_2^{\text{D/L}}/kT \right) g_2(\omega) \right]$$

- The C-term can be calculated with the equations from Barron¹⁰

$$g_j(\omega) = \frac{\omega\Gamma}{(\omega_j^2 - \omega^2)^2 + \omega^2\Gamma^2}$$

$$n'^{\uparrow\uparrow} - n'^{\uparrow\downarrow} = \frac{2\mu_0 c \rho_N B}{3\hbar} \left[\omega_j g_j(\omega) \frac{C_1}{k_B T} - \omega g_j(\omega) \frac{C_2}{k_B T} \right]$$

$$C_1 = \frac{1}{d} \sum_{\alpha, \beta, \gamma} \epsilon_{\alpha, \beta, \gamma} \sum_n m_{n,n}^\alpha \operatorname{Re} \left[\mu_{n,j}^\beta m_{j,n}^\gamma \right]$$

$$C_2 = \frac{\omega}{15d} \sum_{\alpha, \beta} \sum_n m_{n,n}^\alpha \operatorname{Im} \left[3\mu_{n,j}^\beta \Theta_{j,n}^{\beta, \alpha} - \mu_{n,j}^\alpha \Theta_{j,n}^{\beta, \beta} \right]$$

⁹ Barron and Vrbancich, *Molecular Physics* **1984**, 51, 715–730

¹⁰ Barron, *Molecular light scattering and optical activity* **2004** 2nd edition

Vibronic coupling

$$\frac{\partial \theta_{1,2}^e(Q)}{\partial Q_p} = \sum_{k \neq 1} \langle \psi_k^0 | \theta_{1,2}^e | \psi_2^0 \rangle \frac{\partial \langle \bar{\psi}_1^0 | H | \bar{\psi}_k^0 \rangle / \partial Q}{E_1^0 - E_k^0} \\ - \sum_{k \neq 2} \langle \psi_1^0 | \theta_{1,2}^e | \psi_k^0 \rangle \frac{\partial \langle \bar{\psi}_k^0 | H | \bar{\psi}_2^0 \rangle / \partial Q}{E_k^0 - E_2^0}$$

$$\theta_{1,2}^{\text{SO}} = \sum_{k,m} U_{1,k}^{0\dagger} \langle \phi_k | \theta_{k,m}^{\text{SF}}(Q) | \phi_m \rangle U_{m,2}^0$$

- μ : electric dipole moment
- m : magnetic dipole moment
- Θ : traceless quadrupole moment

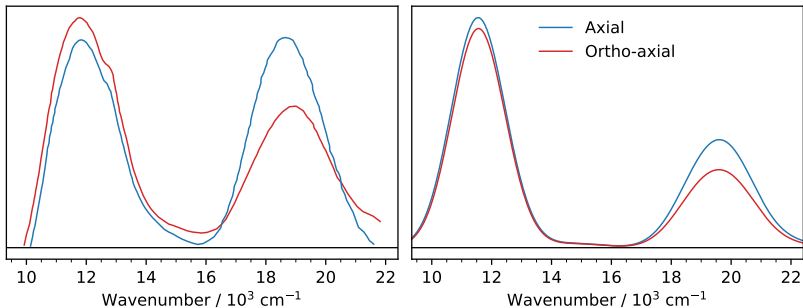
Kohn-Sham Density Functional Theory

- KS-DFT calculations performed with the Gaussian program package
- Optimization and analytical frequency calculations performed with the hybrid B3LYP functional
- A Stuttgart-Dresden-Bonn relativistic ECP and a matching Gaussian-type valence basis set was used for Ni, and the 6-311+G(d) basis for all other atoms
- Wave-function theory calculations were performed on geometries from X-ray crystal structures, followed by optimization of the hydrogen positions with KS-DFT

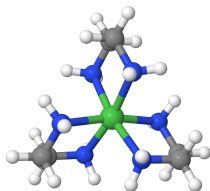
Wave-Function Theory

- Calculations performed within the restricted active space (RAS) framework with a developers version of Molcas/OpenMolcas
- Scalar Relativistic effects were introduced via the second-order Douglass-Kroll-Hess Hamiltonian
- SR spin-free (SF) wavefunctions were determined in state-averaged RASSCF calculations
- Dynamic electron correlation was considered by performing second-order perturbation theory (PT2) calculations
- Spin-orbit coupling introduced via RAS state interaction (RASSI) among the spin-free states
- Diagonal elements of the SF part of the Hamiltonian were ‘dressed’ with PT2 energies

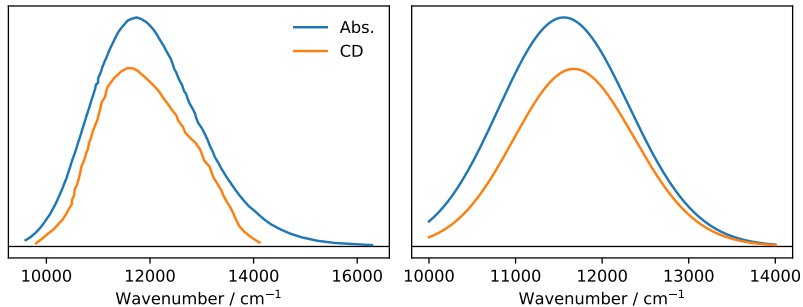
$[\text{Ni}(\text{en})_3]^{2+}$ vibrationally resolved absorption spectrum



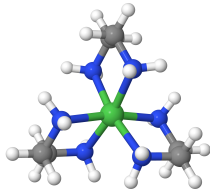
- Calculated (right) agrees well with experimental (left) spectrum in the peak intensity ratios for the peak c.a. 19500 cm^{-1}



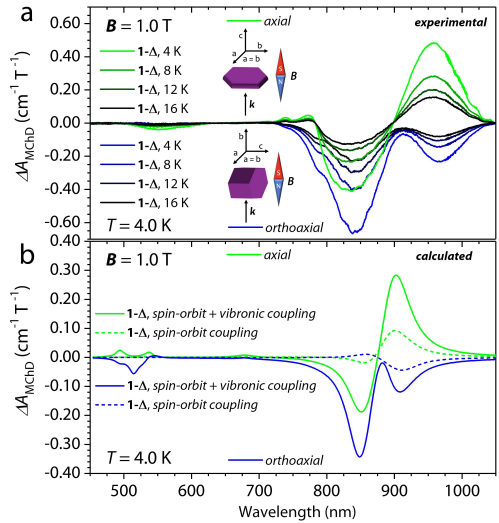
$[\text{Ni}(\text{en})_3]^{2+}$ vibrationally resolved ortho-axial absorption and CD spectrum



- Peak intensity ratios between calculated (right) agrees well with experimental (left) spectrum



$[\text{Ni}(\text{en})_3]^{2+}$ vibrationally resolved MChD spectrum

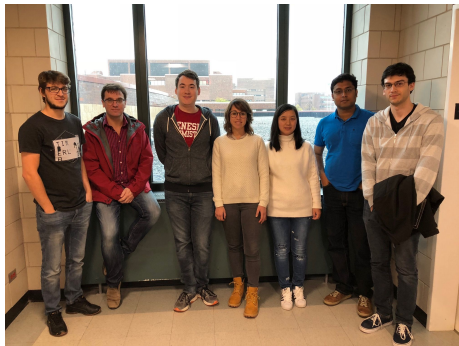


- Calculated (bottom) agrees very well with the experimental (top) spectrum¹¹
- Dashed line shows the purely electronic contributions to the MChD intensities

¹¹ Atzori; Ludowieg; et al, *Sci. Adv.* **2021**, 7

Acknowledgments

- UB center for Computational Research
- Dr. Autschbach and committee
- Autscbach group members



Thank you!

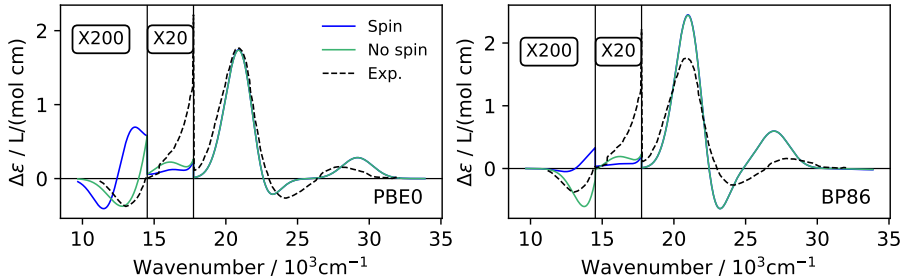
Vibronic coupling approximations

- Normal modes, frequencies and equilibrium structures for the ground and excited states were assumed to be the same
- SO coupling Hamiltonian was calculated with a one-center approximation
- Electron spin contributions vanish as the matrix elements do not depend on vibrational distortions due to the one-center approximation

$[\text{Ni}(\text{en})_3]^{2+}$ active space

- Optimized with a CAS(12,12) made up of 5 $3d$ orbitals, 5 pseudo- $4d$ orbitals, and 2 ligand based orbitals corresponding to the e_g bonding pair in the O_h parentage symmetry
- Wavefunction parameters were generated for a RAS[20,2,2,6,5,5] made up of 6 ligand based orbitals in RAS1, 5 $3d$ orbitals in RAS2, and 5 pseudo- $4d$ in RAS3 generating a total of 40 triplet and 45 singlet states for the d-d and LMCT transitions

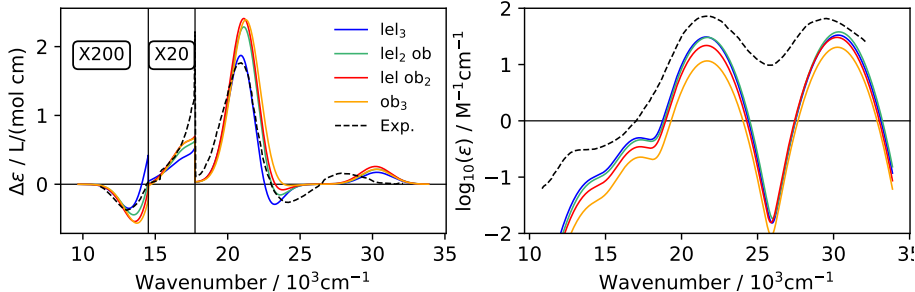
	$(P,\Lambda_{\text{Ir}})\text{-}\mathbf{A}^1$	$(P,\Delta_{\text{Ir}})\text{-}\mathbf{A}^2$	$\Lambda_{\text{Ir}}\text{-}\mathbf{A}$	P-3a	P-3c
Experimental data					
E / eV	2.36	2.36			
	2.21	2.21	2.49	1.91	1.93
	2.04	2.04			
Calcd. TDA-TD-DFT/PBE0					
E / eV^e	2.22	2.22	2.37	1.76	1.79



- $\text{[Co}(\text{en})_3\text{]}^{3+}$ ECD spectra PBE0//B3LYP (left) BP86//B3LYP (right)
- Experimental spectrum (dashed lines) from Mason and Peart¹²
- Energies in the left figure were blue shifted by $\approx 1600 \text{ cm}^{-1}$ (0.2 eV)
- Energies in the right figure were red shifted by $\approx 2400 \text{ cm}^{-1}$ (0.3 eV)
- Used a gaussian broadening of 2500 cm^{-1} (0.31 eV)

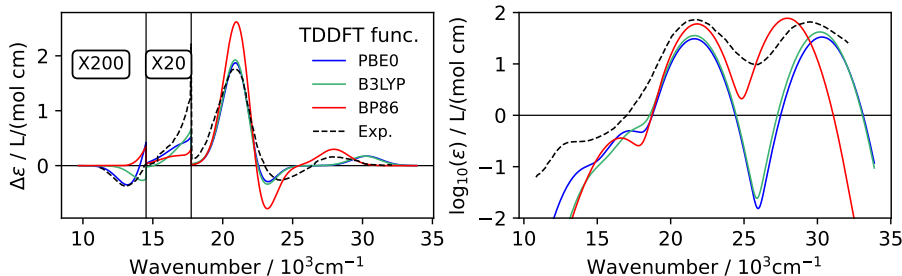
¹² Mason; Peart, *J. Chem. Soc. Dalton Trans* **1977**, 9, 937–941

Conformer effects on $[\text{Co}(\text{en})_3]^{3+}$



- PBE0-TDA//B3LYP

Functional effects on $[\text{Co}(\text{en})_3]^{3+}$



- Blue: PBE0-TDA//B3LYP no shift
- Green: B3LYP-TDA//B3LYP red shift $\approx 950 \text{ cm}^{-1}$ (0.12 eV)
- Red: BP86-TDA//B3LYP red shift $\approx 2400 \text{ cm}^{-1}$ (0.3 eV)

ROA [Co(en)₃]³⁺ ECD

